METEOROLOGICAL OFFICE
-7 DEC1984
LIBRARY
144581

MET O 11 TECHNICAL NOTE NO. 196

SOLUTIONS IN FLOW OVER TOPOGRAPHY USING A GEOMETRIC LAGRANGIAN MODEL

S Chynoweth

Meteorological Office, (Met O 11)
London Road,
Bracknell,
Berkshire
U.K.

N.B. This paper has not been published, permission to quote from it must be obtained from the Assistant Director of the above Meteorological Office Branch.

November 1984

Met O 11 Technical Note no. 196

Solutions in flow over topography using a Geometric Lagrangian Model.

Summary

The Geometric Lagrangian Method (Chynoweth 1984) is extended to a problem on a non-convex domain with general data. The algorithm is then applied to a case study of frontal flow across the Alps.

1. INTRODUCTION

In this paper, the algorithm described in Chynoweth (1984) (hereafter referred to as "C") will be extended to consider the case of two-dimensional frontal flow over topography. The model is essentially a two dimensional Lagrangian conservation form of the Semi-Geostrophic Equations. These are solved by geometric construction.

Under certain restrictions, the Primitive Equations can also be modelled using this method. This involves calculating a correction to the momentum of an element from its horizontal acceleration. The restrictions are imposed by stability considerations.

The algorithm was applied to a case involving the passage of a cold front across the Alps after Buzzi and Tibaldi (1978) (hereafter referred to as BT). The case was actually a study of cyclogenesis and so not all aspects of the motion could be modelled with a two dimensional method. The data was extracted from vertical cross-sections reproduced in the paper.

The incorporation of the topography into the model is by a method which acts on the mass conservation properties of the flow, yet permits fluid to travel through the mountain. This "porous" representation was chosen in preference to a barrier due to the non-uniqueness of the solution if the mountain is impermeable and the extremely non-trivial logic which results. However some justification can be made for this model which will be given later.

The method can be considered in several natural sections. Firstly the discretisation of the data into piecewise constant elements will be described. Following this will be the first guess procedure, the geometric construction involving the topography and the iteration towards the correct

solution. Two ways of inserting the neglected terms to give solutions to the Primitive Equations will be described. Finally the results from the experiments will be discussed.

2. DATA DISCRETISATION

In contrast to standard Eulerian or semi-Lagrangian numerical methods, the geometric method is totally Lagrangian. Therefore, instead of considering a spatial distribution of fluid properties, it is important to look at the conserved quantities of individual fluid parcels (namely the potential temperature θ, the absolute momentum M and the area A). The geometric algorithm requires these three quantities to be prescribed for each fluid element. Following an Eulerian inspired philosophy one would discretise over A by sectioning the initial field into elements of uniform area, and then calculate relevant values of M and θ. A more Lagrangian approach, and the one which is followed, is to uniformly partition the M and θ fields and then to calculate the area of fluid appropriate to each pair (Mi, θi). This can be done since dynamical stability requires M and θ to be monotone in x and z respectively.

Thus consider a vertical cross-section through the atmosphere described in the usual sense by the coordinates (x,z). Let Ω^C be a convex region within this cross-section which includes the topography. Ω^T is a cross-section through the topography in the same plane as Ω^C such that

$$\Omega^T \subset \Omega^C$$

Ω^T will be approximated to be a rectangle of area equal to the mountain cross-section for ease of computation. It will be seen that only the volume of the mountain is important if it is treated as porous.

Let the region in (x,z) space over which the problem is considered be

$$\Omega = \Omega^C \setminus \Omega^T \quad \text{(see figure 1)}$$

For each $\underline{x} \in \Omega$, there exists some

$$\underline{G} = (M(\underline{x}),\ \theta(\underline{x}))$$

Define $\Gamma = \{\underline{y} | \underline{y} = (M(\underline{x}),\ \theta(\underline{x}))$ for some $\underline{x} \in \Omega.\}$

Since $\frac{\partial M}{\partial x} \geq 0$ and $\frac{\partial \theta}{\partial z} \geq 0$, define $G^{-1}: \Gamma \rightarrow \Omega$

The piecewise constant discretisation of Γ takes place as follows. Uniformly partition Γ into N rectangular segments, g_i say, ascribing to each element the (M,θ) value of its centroid. Map g_i into Ω and calculate

$$A_i = \int\int_{G^{-1}(g_i)} dxdz$$

This defines a set $\{ \langle M_i, \theta_i, A_i \rangle |\ i=1,..,N \}$ as required by the algorithm. See figure 1.

(BT) describes a case study of cyclogenesis in the lee of the Alps in April 1973. An active depression moved eastwards from the British Isles to the Baltic with a trailing cold front moving across the Alps ahead of a cold northwesterly airstream (see figures 2, 3). Cyclogenesis occurs at the front as it crosses the Alps, eventually developing into a cutoff mid tropospheric depression.

Vertical cross sections perpendicular to the front are produced using data interpolated from nearby upper air stations (figure 4, 5). These show potential temperature and the normal wind component in knots. The absolute momentum field is easily derived using the expression

$$M = v + fx,$$

where v is the normal wind component in ms^{-1} and f is the Coriolis parameter (taken as $10^{-4}s^{-1}$).

Ω was then partitioned by inspection into N elements $\{\Omega_i \mid i=1,..,N\}$, of uniform intervals in (M,θ) except at the boundaries where some representative value was chosen. Similarly in the neigbourhood of the tropopause very little change in the fields takes place and thus a coarser subdivision is used.

3. FIRST GUESS PROCEDURE

Given $\{\langle M_i,\theta_i,A_i\rangle \mid i=1,..,N\}$, we require a set $\{s_i \mid i=1,..,N\}$ such that if

$$\phi(x,z) = \max_{1\leqslant j\leqslant N} \{ xM_j + z\theta_j + s_j \} \qquad (1)$$

then $\phi(x,z) = x M_i + z\theta_i + s_i \iff (x,z) \in \Omega_i$

In order to construct the correct convex shell (1), the iteration requires a first guess sufficiently close to the solution. Due to the more general nature of the data, the analytic first guess described in (C) is no longer useful.

A multigrid procedure is used based upon successive refinement of the (M,θ) grid.

Γ is initially divided into two segments

$$g_{11} = \{ (M,\theta) \in \Gamma \mid M < M' \}$$

$$g_{12} = \{ (M,\theta) \in \Gamma \mid M \geqslant M' \}$$

for some central M'.

These correspond to two "macro elements"

$$\Omega_{11} = G^{-1}(g_{11}) = \bigcup_{M_i<M'} \Omega_i$$

$$\Omega_{12} = G^{-1}(g_{12}) = \bigcup_{M_i \geqslant M'} \Omega_i$$

The values of momentum and temperature for the two macro-elements are obtained by area-averaging the gradients of the basic elements contained within them. This two element problem over Ω can then be trivially solved using a simple iteration to obtain a difference in s between the two elements.

g_{11} and g_{12} are then subdivided:

$$g_{21} = \{ (M,\theta) \in g_{11} \mid \theta < \theta' \}$$

$$g_{22} = \{ (M,\theta) \in g_{11} \mid \theta \geq \theta' \}$$

$$g_{23} = \{ (M,\theta) \in g_{12} \mid \theta < \theta' \}$$

$$g_{24} = \{ (M,\theta) \in g_{12} \mid \theta \geq \theta' \}$$

for some central θ'.

Defining $\Omega_{2i} = G^{-1}(g_{2i})$ for i=1,2,3,4 one obtains two more two element problems. These are solved over Ω_{11} and Ω_{12} respectively. This recursive procedure continues until no more subdivision is possible. The resulting set $\{ s_i \mid i=1,..,N \}$ will not be an exact solution to the problem as the boundaries between the macro elements are not modified after the next subdivision problem is solved. However the result should be close enough to the final solution to act as a first guess for an iteration based upon a linearization of the problem which will be described later.

4. GEOMETRIC CONSTRUCTION

Given the set $\{ s_i^r \mid i=1,..,N\}$ and $\{\langle M_i,\theta_i,A_i\rangle : i=1,..N\}$, the convex shell

$$\phi^r(x,z) = \max_{1\leq i\leq N} (xM_i + z.\theta_i + s_i^r)$$

is constructed as described in (C). For ease of computation this procedure acts on a rectangular domain and so we first consider the shell over the whole of Ω^C, that is ignoring the mountain. Certain fluid elements will

now lie wholly or partly in Ω^T. Consider such an element, Ω_j, where $\Omega^T \cap \Omega_j \neq \phi$.

In the case where no topography is present, the area of an element Ω_i^r, is calculated on the rth construction:

$$A_i^r = \int\int_{\Omega^r i} dxdz$$

and then $\{s_i^r : 1 \leq i \leq N\}$ is adjusted such that $A_i^r \to A_i$ as r increases.

In the topography case we redefine

$$A_j^r = \int\int_{\Omega_i^r} dxdz - \int\int_{\Omega_j^r \cap \Omega^T} dxdz$$

and iterate over these areas.

It is this method which regards the mountain as porous. Standard theory shows (Cullen and Purser 1984) that the uniqueness of the solution breaks down if the domain is non-convex as here in the presence of a mountain. In order to make the solution unique, extra conditions are required. The simplest of these is to allow motion "through" the mountain. This means that fluid cannot be trapped by orography which is the situation that gives multiple solutions.

In a two dimensional model of flow across a mountain range, this approximation has some justification. Standard two dimensional mountain models act as a complete block to the flow for some vertical barrier of height roughly equal to the mean orographic height. This does not realistically permit flow through valleys or round the mountain range as happens in practice. However blockng of flow is still an important mechanism and is completely ignored if the mountain is treated as porous. The most realistic represntation would be a combination of the two

extremes. The mountain would be solid up to a height representative of the altitude of the valleys and porous above, representing the mass conservation but not the blocking effects of individual peaks.

Work is in progress to model a solid mountain range, and this will be described at a later date.

5. ITERATIVE SCHEME

After the rth iteration of the shell, assume the areas obtained are not correct to within sufficient accuracy, ie.

Given ϵ, there exists $i \in 1,..,N$ such that $|A_i^r - A_i| > \epsilon$, then one must correct the set $\{s_i^r \mid i=1,..,N\}$ such that $A_i^r \to A_i$ for all i.

For ease of notation, define the following:

$$\underline{A}^r = (A_1^r, A_2^r, \ldots, A_N^r)$$

$$\underline{A} = (A_1, A_2, \ldots, A_N)$$

$$\underline{s}^r = (s_1^r, s_2^r, \ldots, s_N^r)$$

$$\underline{s} = (s_1, s_2, \ldots, s_N)$$

Then for $\underline{s}^r$ sufficiently close to $\underline{s}$

$$\underline{A}^r - \underline{A} = ((\partial Ai/\partial s_j))\,(\underline{s}^r - \underline{s}) \qquad (2)$$

Initially the segmenets are adjusted until all elements are represented in Ω, ie $A_i^r \neq 0$ for any i=1,..,N. When this is the case, the linearized equation (2) is used to define $\underline{s}^{r+1}$. This is done as follows: When constructing an element, Ω_i say, the length l_{ij} of an edge with any neighbour Ω_j is easily found. In order to obtain $\partial A_i/\partial s_j$ we also require the distance δ_{ij} which the edge $\Omega i n \Omega j$ moves perpendicular to itself when s_i is incremented by Δs_i say.

Define a vector $\underline{r}$ in the (x,z) plane, perpendicular to $\Omega i n \Omega j$ (see figure 6a). The gradient of $\Omega i n \Omega j$ is given by:

$$\left.\frac{\partial z}{\partial x}\right|_{\Omega_i n \Omega_j} = -\frac{(Mi - Mj)}{(\theta i - \theta j)} \qquad \text{(see C)}$$

let $\underline{r} = \frac{\theta_i - \theta_j}{M_i - M_j}\underline{k} + \underline{i}$

If $r = x.|\underline{r}|$ defines a component in the direction of $\underline{r}$, then let

$$\frac{\partial \phi_i}{\partial r} = \tan \alpha$$

$$\frac{\partial \phi_j}{\partial r} = \tan \beta$$

From figure 6b: $\tan \alpha = \frac{\Delta si + a}{\delta_{ij}}$

$$\tan \beta = \frac{a}{\delta_{ij}}$$

$$\therefore \quad \delta_{ij} = \frac{\Delta s_j}{\tan\alpha - \tan\beta}$$

Let $\Delta A_i = l_{ij}.\delta_{ij}$

$$\frac{\partial \phi_i}{\partial r} = \frac{\partial \phi_i}{\partial x}.\frac{dx}{dr} + \frac{\partial \phi_i}{\partial z} . \frac{dz}{dr}$$

$$= M_i . \frac{1}{|\underline{r}|} + \theta_i \frac{(\theta_i - \theta_j)}{(M_i - M_j)} . \frac{1}{|\underline{r}|}$$

since $M_i = \frac{\partial \phi_i}{\partial x}$ and $\theta_i = \frac{\partial \phi_i}{\partial z}$ (see C)

Therefore $\tan \alpha = \frac{M_i (M_i - M_j) + \theta_i (\theta_i - \theta_j)}{(M_i - M_j) .|\underline{r}|}$

and similarly $\tan \beta = \frac{M_j (M_i - M_j) + \theta_j (\theta_i - \theta_j)}{(M_i - M_j).|\underline{r}|}$

The approximation is made

$$\frac{\partial A_j}{\partial s_j} \simeq \frac{\Delta A_j}{\Delta s_j} \qquad \text{for } i \neq j$$

$$\frac{\partial A_i}{\partial s_i} = - \sum_{i=j} \frac{\partial A_j}{\partial s_i}$$

and for elements with no common boundary

$$\frac{\partial A_j}{\partial s_j} = 0 \qquad \text{for } i \neq j$$

The errors in this approximation arise because as one element moves with respect to another, the boundary lengths change (see figure 6a) and also the neighbours themselves change, introducing non linearity into the problem.

From (2), $\underline{s}^{r+1}$ is given by

$$\underline{A}^r - \underline{A} = ((\partial A_i/\partial s_j))\,(\underline{s}^r - \underline{s}^{r+1})$$

ie. $$\underline{s}^{r+1} = \underline{s}^r - ((\partial A_i/\partial s_i))^{-1}\,(\underline{A}^r - \underline{A})$$

which is solved using a Numerical Algorithms Group routine. The iteration is repeated until for some predefined ϵ, $||\,A^r - A||_\infty < \epsilon$.

6. PRIMITIVE EQUATION CORRECTION

Previously we have used the model to solve the Lagrangian Geostrophic Momentum Equations without the presence of any forcing:

$$\frac{DM}{Dt} = 0$$

$$\frac{DA}{Dt} = 0 \qquad (3)$$

$$\frac{D\theta}{Dt} = 0$$

$$\frac{\partial\phi}{\partial x} = M\,,\quad \frac{\partial\phi}{\partial z} = \theta,\quad \phi = \phi_g + {}^1/_2\, fx^2$$

where $M = v + fx$, v is the long front wind component, f is the Coriolis parameter, ϕ_g is the geopotential and A is the area of a fluid element.

The full Primitive Equations imply (From Hoskins 1975)

$$u = u_g - \frac{1}{f}\dot{v}_g - \frac{1}{f^2}\ddot{u}_g + \frac{1}{f^3}\dddot{v}_g + \qquad (4)$$

$$v = v_g + \frac{1}{f}\dot{u}_g - \frac{1}{f^2}\ddot{v}_g - \frac{1}{f^3}\dddot{u}_g + \ldots \qquad (5)$$

$$= v_g + v'$$

If $M_g = v_g + fx$ then

$$M_g = M - v'$$

$$\frac{DM_g}{Dt} = -\frac{Dv'}{Dt} \quad \text{from (3)}$$

$$\frac{DM_g}{Dt} = -\frac{D}{Dt}\left(-\frac{1}{f}u_g - \frac{1}{f^2}v_g + \ldots\right)$$

$$\frac{DM_g}{Dt} = -\frac{D}{Dt}\left(\frac{1}{f}\frac{Du}{Dt}\right) \quad \text{from (4)}$$

Let x_i represent the position of a fluid particle at some time to + $i\Delta t$, then let

$$\Delta M = \frac{-1}{f(\Delta t)^2} (X_3 - 4x_2 + 4x_1 - x_o)$$

Then $$\left.\frac{DM_g}{Dt}\right|_{t=t_o + \frac{3\Delta t}{2}} \simeq \frac{\Delta M}{\Delta t}$$

Extending this approximation to other time steps, write

$$M_g \Big|_{t=to+i\Delta t} = i\Delta M + M_g|_{t=to} \quad \text{for } i=1,2,3$$

Considering theoretical stability requirements, the change in position of a particle due to its change in momentum ΔM is approximately $f^{-1}\Delta M$. The actual acceleration of a particle gives it a displacement of

$$\Delta x = x_{3/2} - 4x_{1/2} + 4x_{-1/2} - x_{-3/2} = -f\,(\Delta t)^2\,\Delta M.$$

For stability of the method, we require

$$|\,f^{-1}\,\Delta M| < |\,-f\,(\Delta t)^2\,\Delta M|$$

$$f^2\,\Delta t^2 > 1$$

$$\Delta t > f^{-1} \simeq 3 \text{ hours}$$

However the numerical method of solving the problem introduces further errors, so that a more stringent criterion is needed. The movement of an element is not inherently well defined due to the variation in shape of the element. Accordingly one considers the displacement of its centroid.

Given two neighbouring elements Ωi, Ωj, of momentum values M_1 and M_2, suppose these are subjected to changes ΔM_2, and ΔM_2 respectively.

If $M_2 + \Delta M_2 < M_1 + \Delta M_1$

and $M_2 > M_1$

then Ω_i and Ω_j will change places. If Δh is some measure of the difference in widths between the two elements, then the element can move $f^{-1}\Delta M \pm \Delta h$ due to a change of ΔM in the momentum.

Thus, revising the previous stability criterion,

$$|f^{-1}\,\Delta M(1 + \frac{\Delta h}{\Delta x})| < |f(\Delta t)^2\,\Delta M|$$

$$|f^2\,(\Delta t)^2| > 1 + \Delta h/\Delta x$$

$$\Delta t > f^{-1}.(1 + \Delta h/\Delta x)^{1/2}$$

However due to the variability of the element shape, Δh cannot be predetermined. In practice the stability criterion for the data used was

$$\Delta t > 2f^{-1} \simeq 6 \text{ hours}$$

A more physical interpretation of the above is that the primitive equation solution will contain lee waves. The semi-geostrophic solution imposes a dynamical stability condition on the geostrophic wind rather than the actual wind, which is inappropriate if there are waves present.

By calculating the changes in M_g implied by the derived accelerations Du/Dt on short time scales, we can deduce the changes in the slopes of the pressure surfaces which would be associated with lee waves. However the dynamical stability condition on the actual wind must still be satisfied, so we assume that the only effect of the waves is to change the shape of interelement boundaries without needing any rearrangement of the elements. Thus in method (PEI), the gradients of element boundaries are recalculated using corrected values of momentum. These are overlayed on the Semi-Geostrophic solution in order to demonstrate which elements undergo large accelerations causing lee-wave activity.

(PEII) operates only on the longer time scales greater than $2f^{-1}$. A six hour timestep is used and the solution is allowed to converge to one satisfying the convex stability condition.

7. RESULTS

The initial distribution of the thirty six fluid elements derived from the cross section is shown in figure 7. Results are accurate to within approx 1.25% of the smallest area. Table 1 shows the initial values of M and θ which remain constant except in the Primitive Equation case where M is adjusted. As can be seen from the table, except for those elements at the tropopause, namely Ω_1, Ω_2 and Ω_3, elements take values of θ varying uniformly in the vertical. Therefore all non-vertical lines within Ω in figure 7 can be considered as unsmoothed approximations to isotherms at 10° intervals. Figure 8 shows the wind field parallel to the front in ms^{-1}. This was derived by calculating, for each element Ω_i, with centroid x_i

$$v_i = M_i - f.x_i$$

The contour map is a bicubic spline over the resulting irregular grid of thirty-six points. Comparisons of this field with the initial velocity field from which the data is derived should be made with caution due to the differences in the derivation of data and results. The restriction from the velocity and temperature fields to piecewise constant data was ad hoc and somewhat qualitative. The prolongation was interpolation over a sparse mesh.

7.1 Semi Geostrophic Model

Figures 9(a and b) and 10(a and b) show the results from the Semi-Geostrophic scheme after six and twelve hours respectively. No large effects of the topography on the flow are demonstrated since the mountain does not block flow through it. However a local steepening of the frontal surface can be recognised. Over the first six hours (figure 7 and 9(a)), the region of fluid represented by Ω_{30} descends as it moves past the mountain. Meanwhile Ω_{29} rises, not because it cannot flow through the

topography but beause it cannot remain within it. If the mountain formed a solid barrier, Ω_{36} would have been forced to rise instead of accelerating through the obstruction. The process continues bewteen six and twelve hours as Ω_{28} rises while Ω_{29} descends behind the mountain.

Figures 8, 9b and 10b similarly show little change throughout the twelve hours. A slight reduction in v behind the Alps is noticeable which could be interpreted as a tendency towards a cyclonic circulation. However the effect is too small to draw any conclusions.

7.2 Primitive Equation Correction

Figures 11 and 12 show the results after six and twelve hours from PEI. Downstream of the mountain, acceleration of the fluid has caused large adjustments of absolute momentum, demonstrated by the changes in element boundaries. The acceleration is primarily caused when an element, or part of an element, moves instantaneously from one side of the mountain to the other. This has some physical validity as sudden adjustments of this type take place in reality, causing very strong winds through mountain valleys.

PEII (figures 13(a&b) and 14(a&b)) show results similar to those of the Semi-Geostrophic solution. However differences are apparent downstream, and immediately surrounding the mountain where acceleration terms are important. A comparison of figure 14(b) with figure 10(b) shows stronger horizontal gradients in the velocity field behind the mountain, implying a greater tendency towards a downwind circulation.

8. CONCLUSION

The Geometric Method provides a useful method of studying flows such as the one considered above.

The results demonstrate the steepening of the frontal surface as it crosses the topography. However features in figure 5 such as the retarding of the subsiduary jet and the lower level cold front have not been produced by the model. The conclusion is that while the mass conservation effect of the mountain is important, the blocking effect and, in this case, the three dimensionality of the flow are more so. Therefore incorporating solid topography into the Geometric Method should produce useful results.

Further improvements can be made in the numerical method. A more qualitative derivation of piecewise constant data would improve accuracy and enable better prolongation back to the original fields. Refining the mesh by taking smaller elements would also improve representation. However, elements should not be on scales smaller than those for which Semi-Geostrophic theory is valid in the neighbourhood of the mountain.

REFERENCES

(BT) Buzzi and Tibaldi; "Cyclogenesis in the lee of the Alps: a case study".
Quart. J.R. Met. Soc. April 1978, Vol 104, pp 271-287.

(C) Chynoweth; "Geometric Solutions to the Lagrangian Semi-Geostrophic Equations".
Met O 11 Technical Note No 182, January 1984.

Cullen and Purser; "An Extended Lagrangian Theory of Semi-Geostrophic Frontogenesis".
J. Atmos. Sci. 1984, Vol 41, No 9 pp 1477-1497.

Hoskins; "The Geostrophic Momentum Approximation and the Semi Geostrophic Equations".
J. Atmos. Sci, 1975, Vol 32, No 2, pp 233-242.

TABLE 1

Element	Potential Temperature, θ(K)	Absolute Momentum, M (ms^{-1})
1	345	20
2	345	60
3	335	105
4	320	15
5	320	30
6	320	50
7	320	70
8	320	90
9	320	110
10	320	125
11	310	15
12	310	30
13	310	50
14	310	70
15	310	90
16	310	110
17	310	125
18	300	15
19	300	30
20	300	50
21	300	70
22	300	90
23	300	110
24	300	125
25	290	15

26	290	30
27	290	50
28	290	70
29	290	90
30	290	110
31	290	125
32	280	15
33	280	30
34	280	50
35	280	70
36	280	90

TABLE 2

Contour annotation	Contour value in ms^{-1}
1	-5
2	0
3	5
4	10
5	15
6	20
7	25
8	30
9	35
10	40
11	45

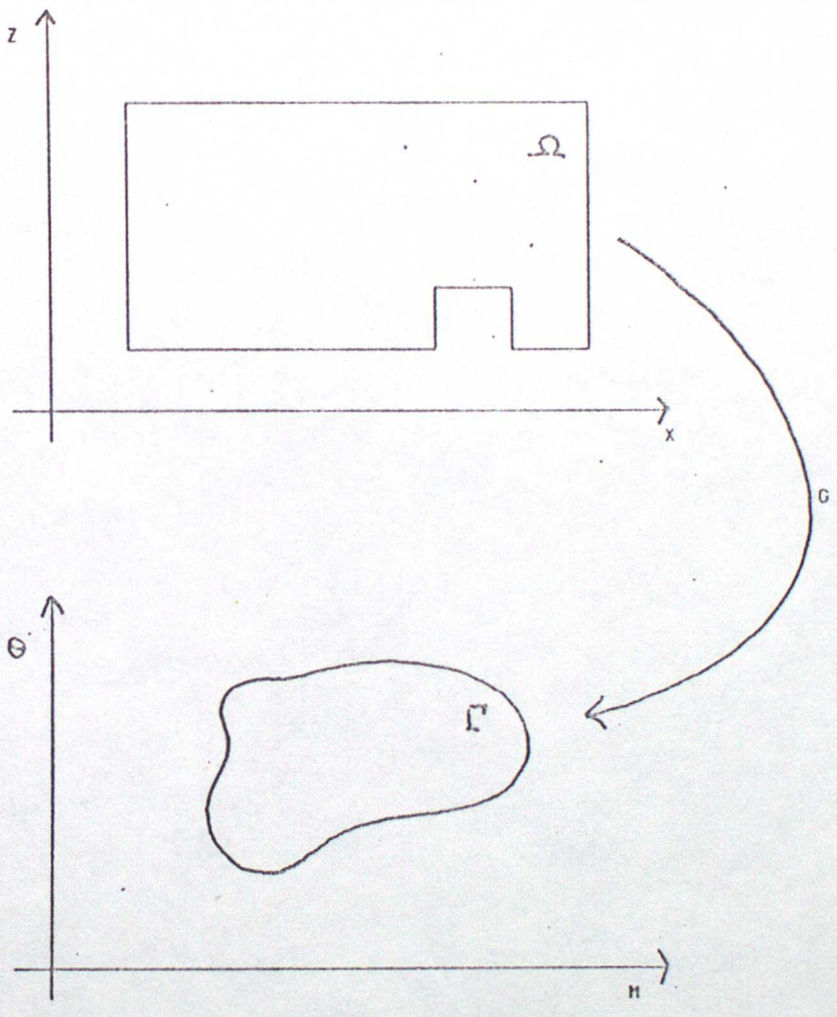

FIGURE 1

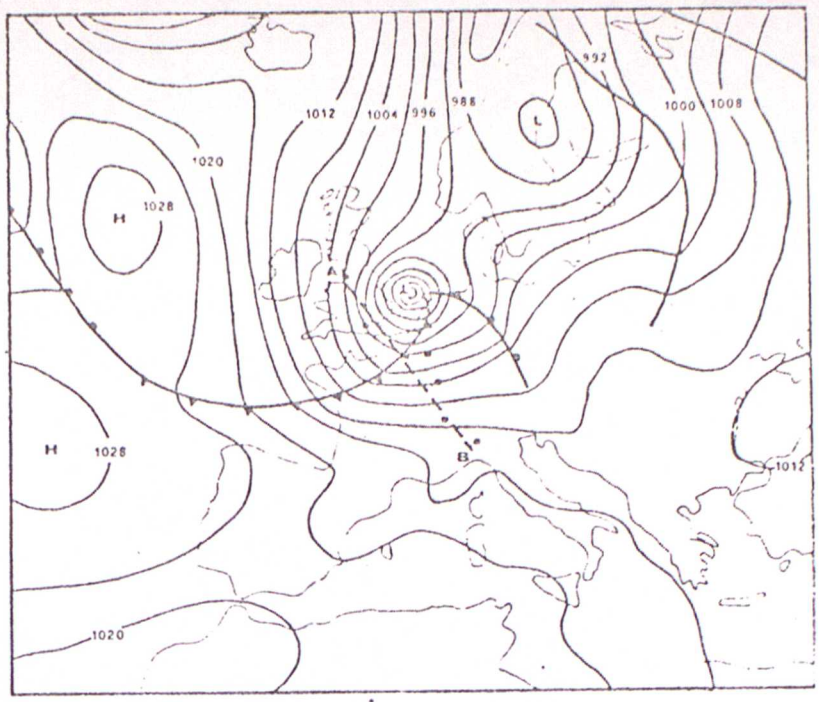

Figure 2: 2 April 1973, 12 GMT. Mean sea level pressure. (After BT).

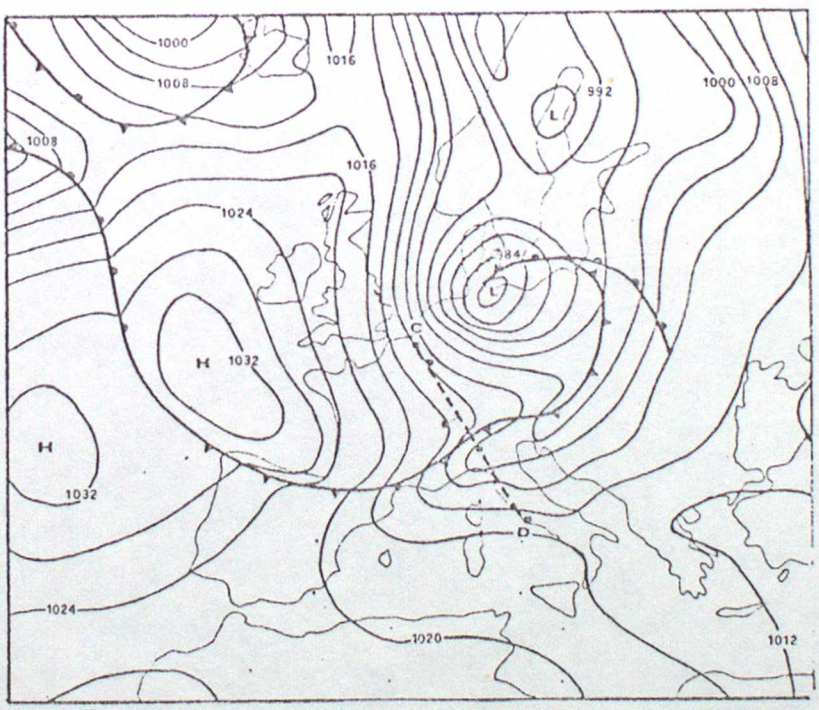

Figure 3: 3 April 1973 00 GMT. Mean sea level pressure (After BT).

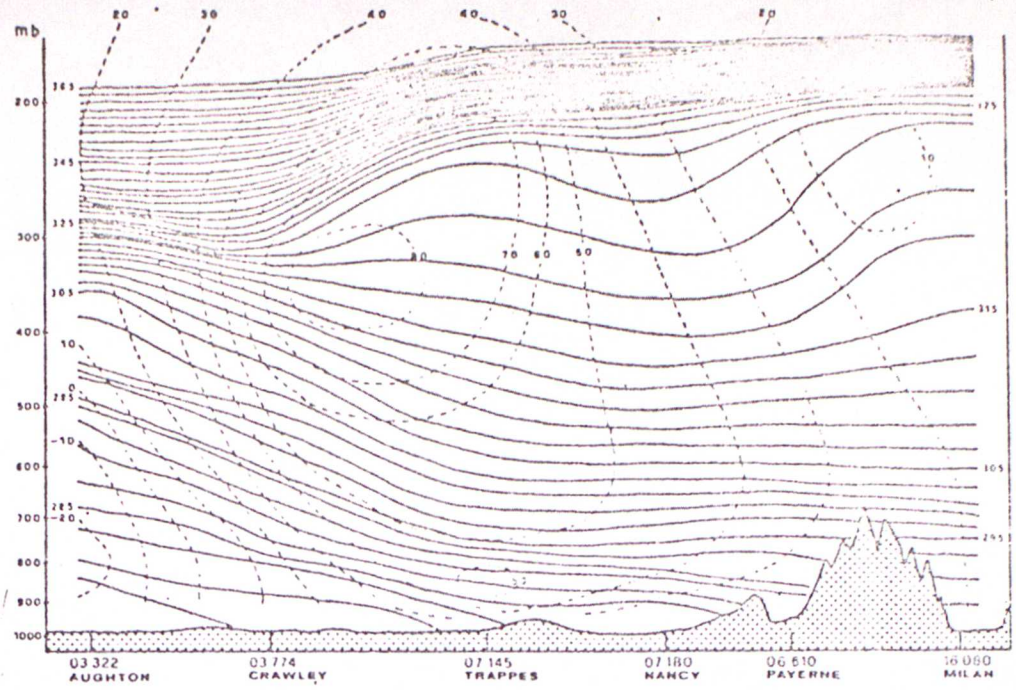

Figure 4: Cross section along the line A-B of figure 2; 2 April 1973, 12 GMT. Full lines: isentropes; dashed lines: normal wind component in knots. (After BT).

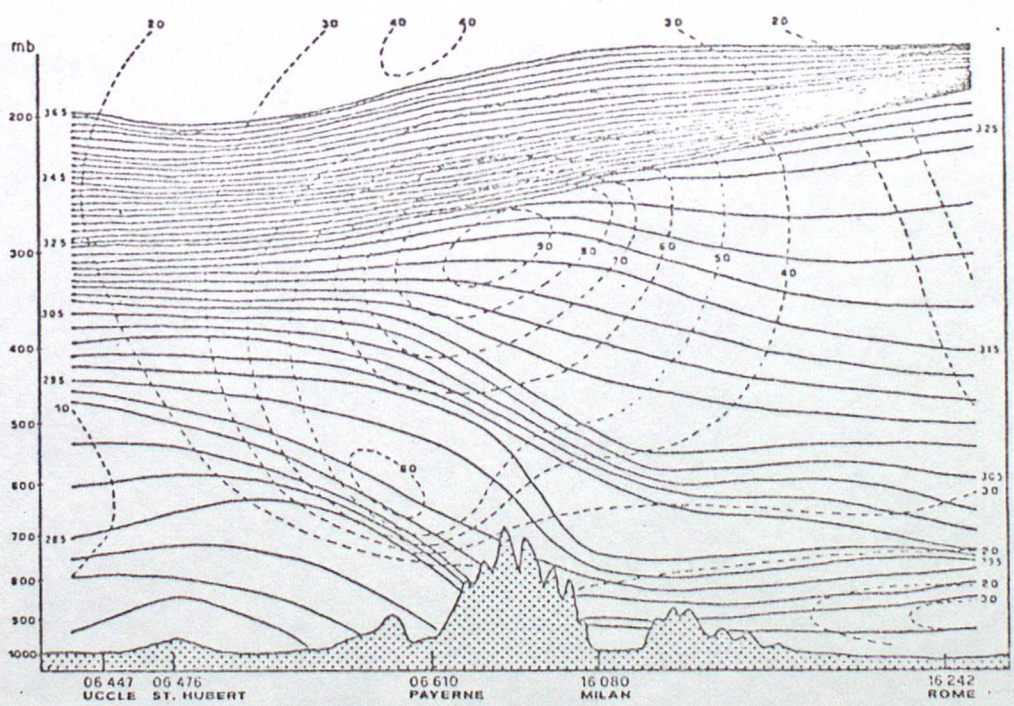

Figure 5: Cross section along the line C-D of figure 3; 3 April 1973, 00 GMT. (See also fig 4).

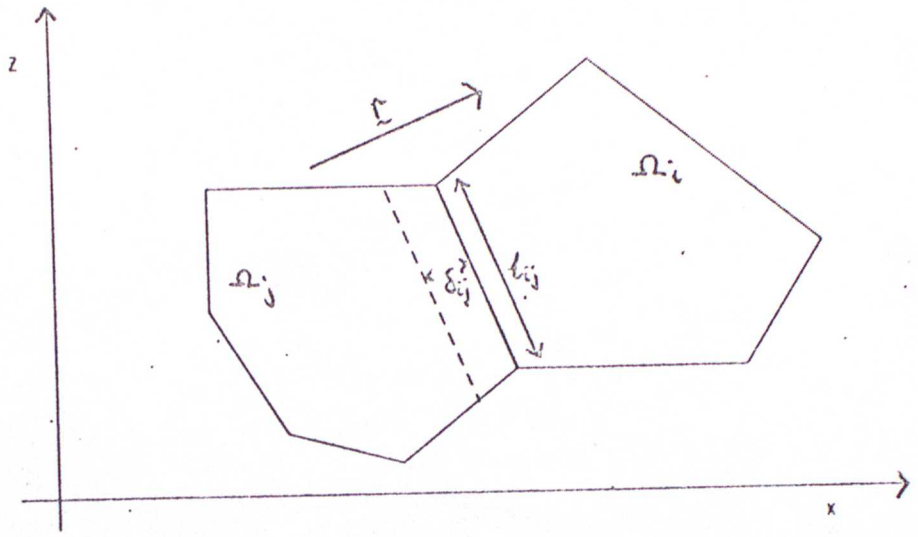

FIGURE 6(A)

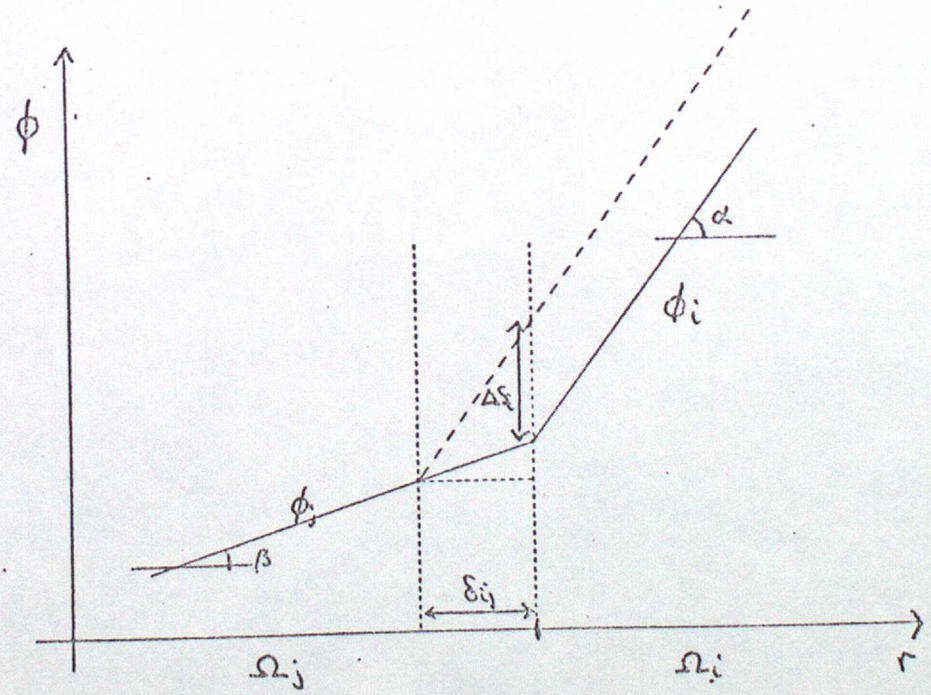

FIGURE 6(B)

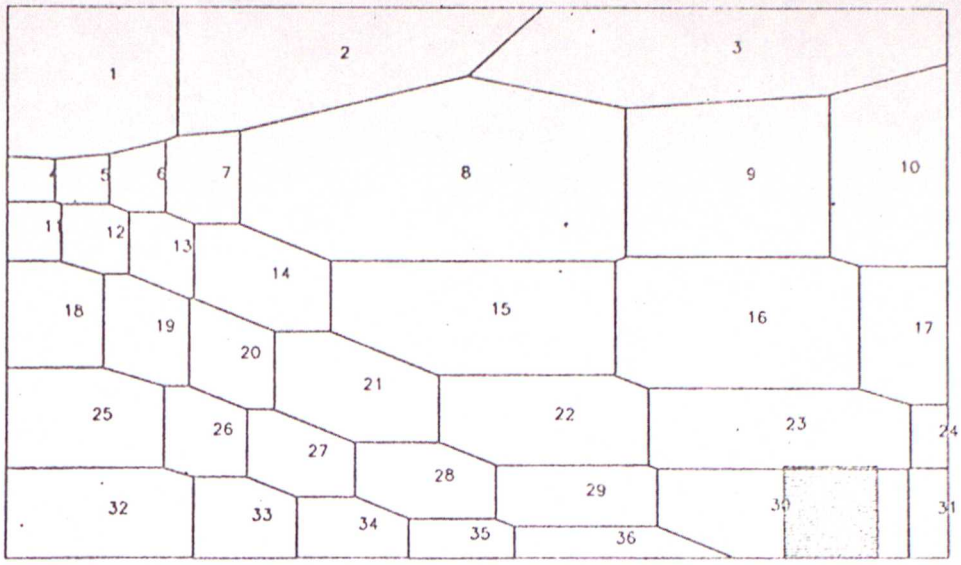

Figure 7: Initial distribution of fluid elements. 2 April 1973, 12 GMT.

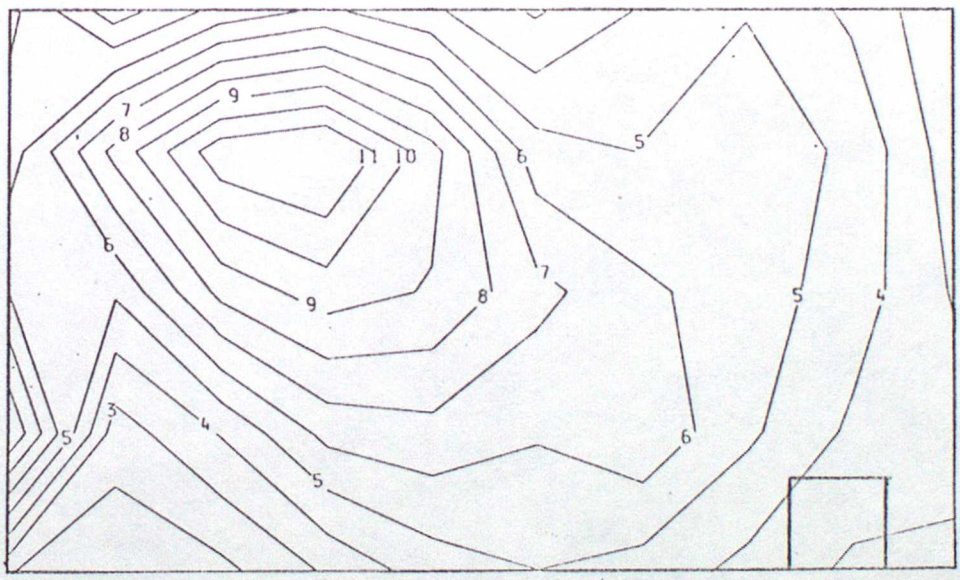

Figure 8: Normal wind component. 2 April 1973 12 GMT. See Table 2 for contour values.

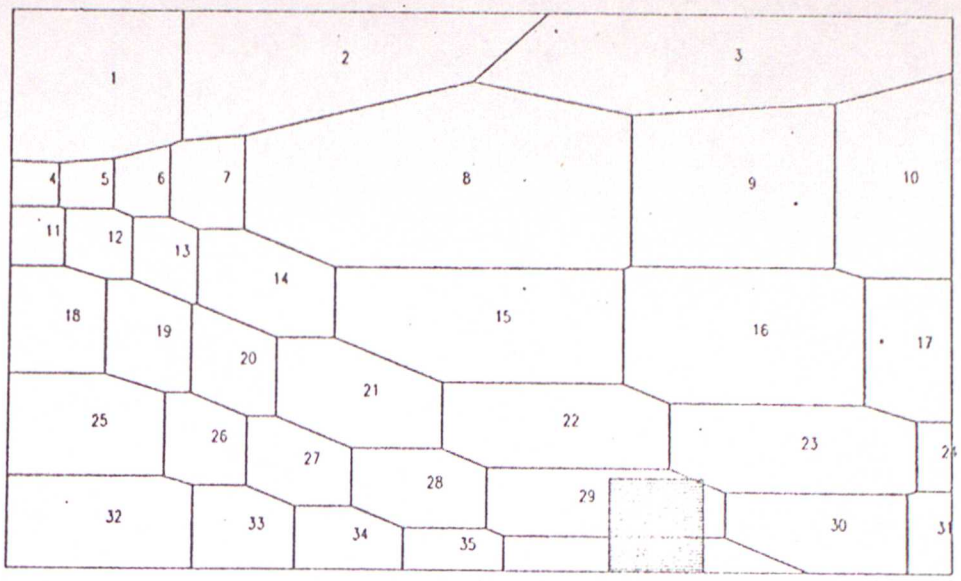

Figure 9(a): Semi-Geostrophic solution. Element distribution 2 April 18 GMT.

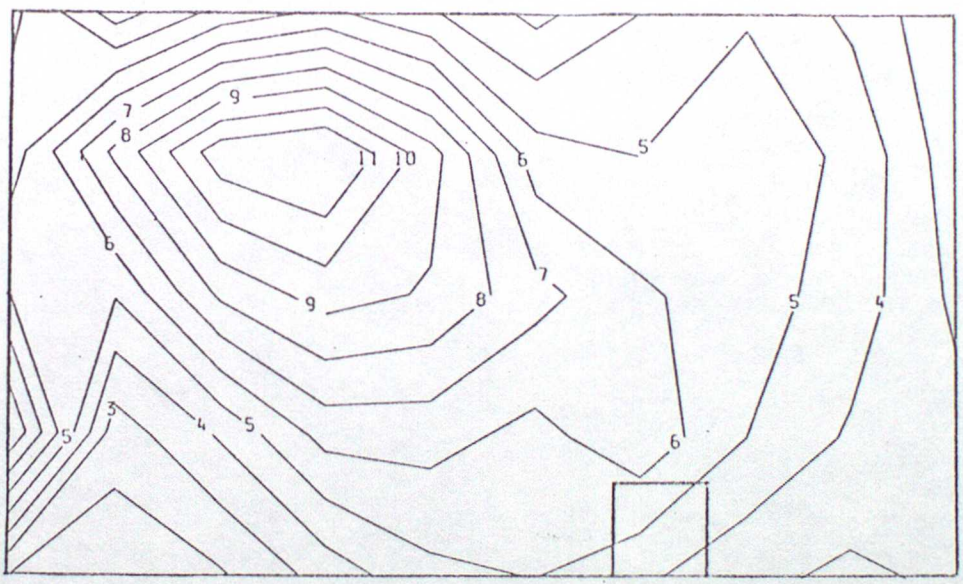

Figure 9(b): Semi Geostrophic solution. Normal wind component 2 April 18 GMT. See Table 2 for contour values.

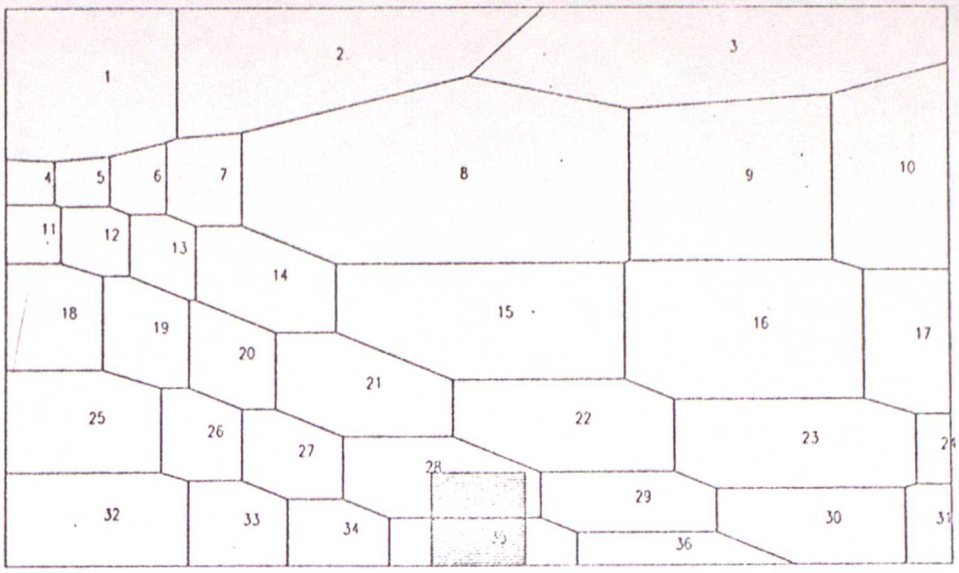

Figure 10(a): Semi-Geostrophic solution. Element distribution 3 April 00 GMT.

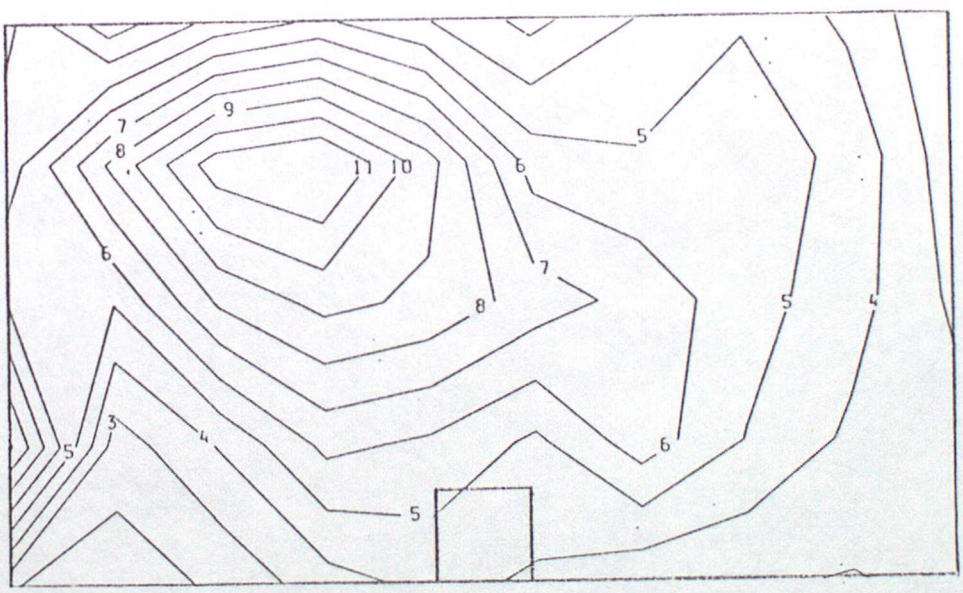

Figure 10(b): Semi-Geostrophic solution. Normal wind component 3 April 00 GMT. See Table 2 for contour values.

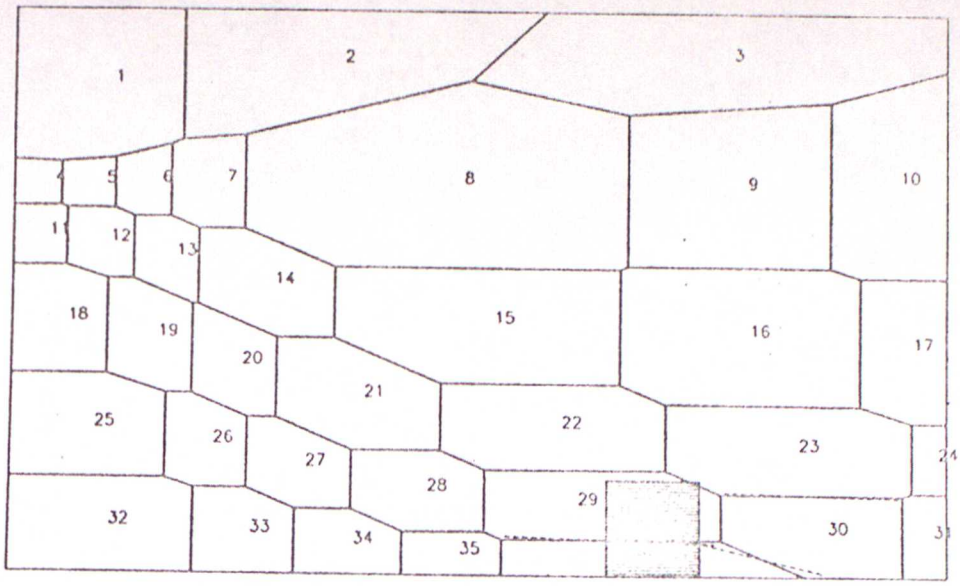

Figure 11. PEI. Element distribution. 2 April 18 GMT Dotted lines: adjusted element boundaries.

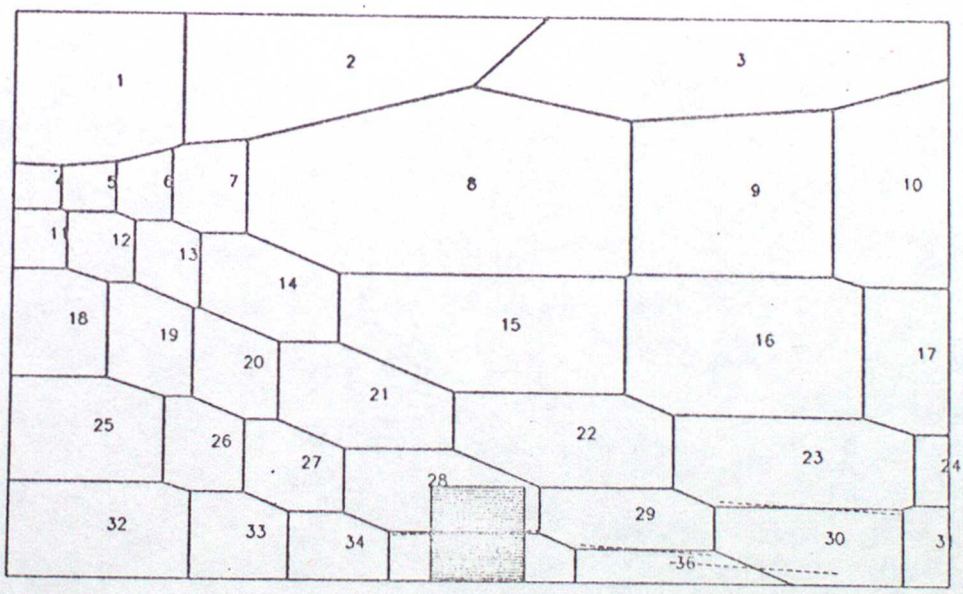

Figure 12. PEI Element distribution 3 April 00 GMT (see also Fig 11).

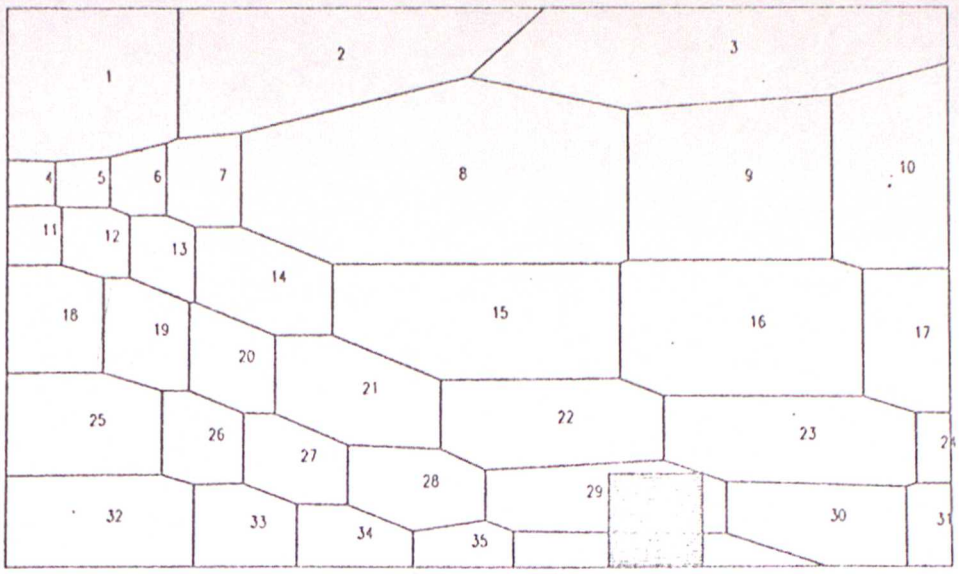

Figure 13(a) PEII Element distribution 2 April 18 GMT

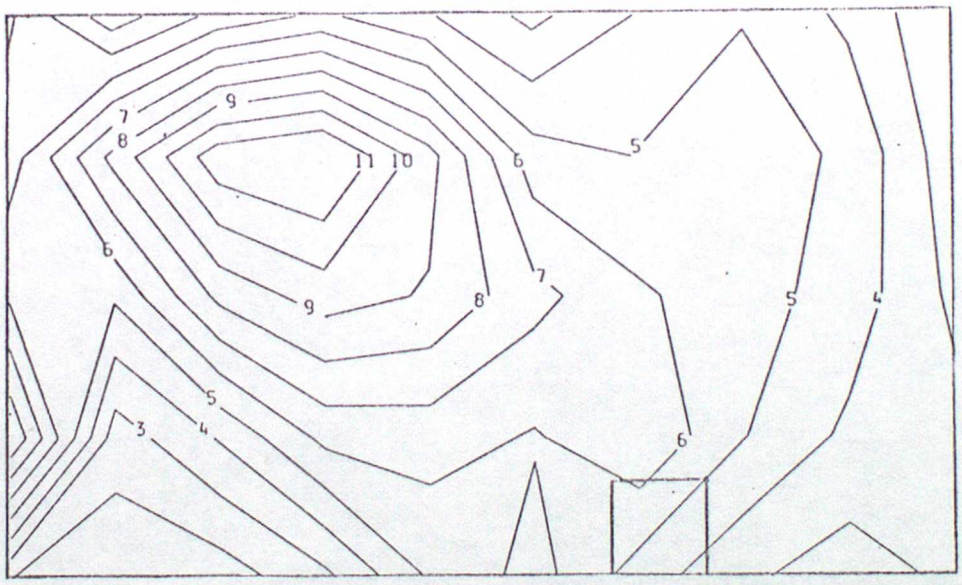

Figure 13(b) PEII. Normal wind component 2 April 18 GMT. See Table 2 for contour values.

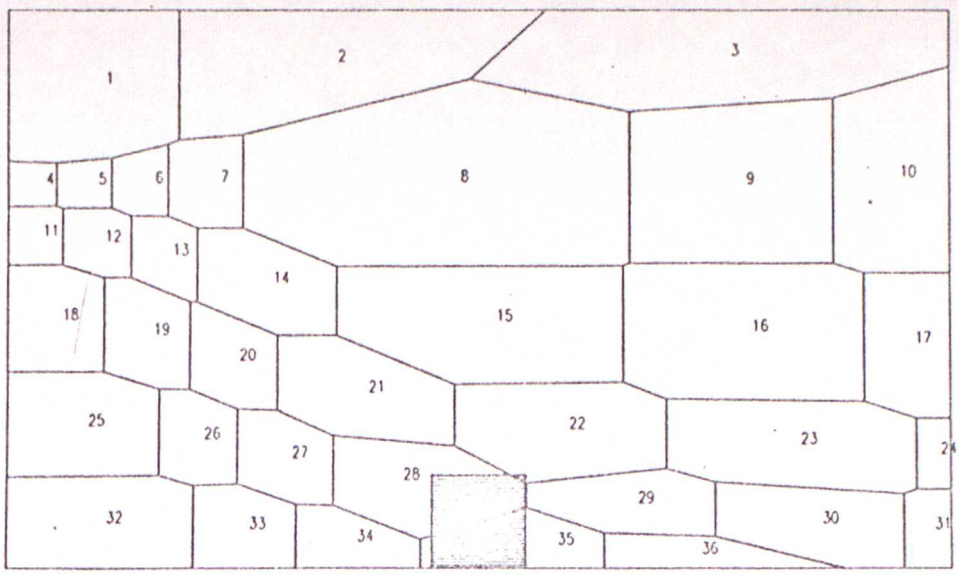

Figure 14(a) PEII. Element distribution. 3 April 00 GMT.

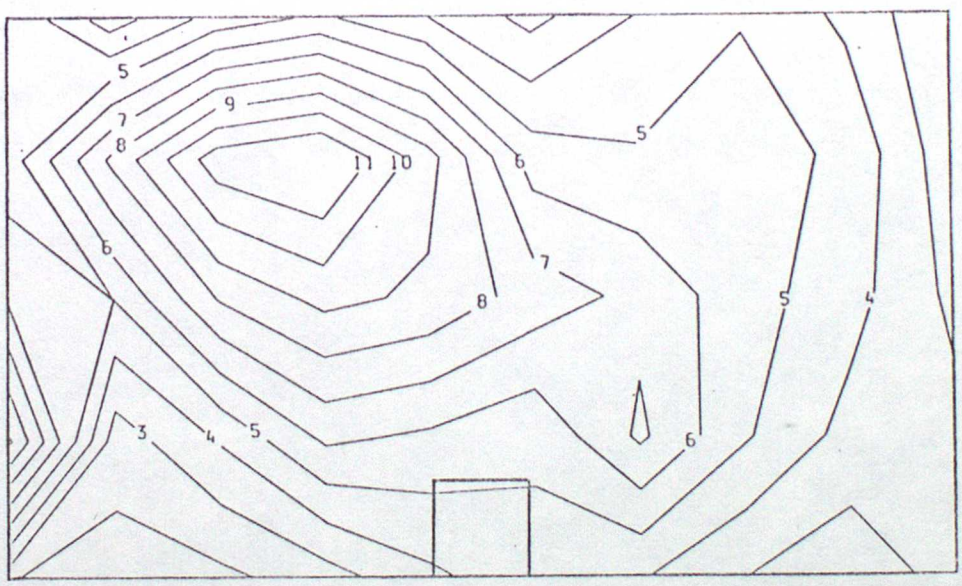

Figure 14(b) PEII Normal wind component 3 April 00 GMT. See Table 2 for contour values.